Lanthanide-Tetrazolate Complexes Combining SIM and Luminescent Properties. The Effect of the Replacement of N_3-tetrazolate by β-Diketonate Ligands on the anisotropy energy barrier

Juan-Ramón Jiménez,[†] Ismael F. Díaz-Ortega,[†] Eliseo Ruiz,[*,#] Daniel Aravena,[¶] Simon J. A. Pope,[‡] Enrique Colacio,[*,†] Juan Manuel Herrera[*,†]

[†] *Departamento de Química Inorgánica, Facultad de Ciencias, Universidad de Granada, Avda. Fuentenueva s/n, 18071, Granada, Spain.*

[#] *Departament de Química Inorgànica and Institut de Recerca de Química Teòrica i Computacional, Universitat de Barcelona, Diagonal 645, 08028, Barcelona, Spain.*

[‡] *Cardiff School of Chemistry, Cardiff University, Cardiff, CF10 3AT, UK.*

[¶] *Departamento de Química de los Materiales, Facultad de Química y Biología, Universidad de Santiago de Chile (USACH), Casilla 40, Correo 33, Santiago Chile*

ABSTRACT

Three new sets of mononuclear Ln^{III} complexes of general formulas $[LnL_3]\cdot CH_3OH$ (Ln^{III} = Yb (**1**), Er (**2**), Dy (**3**), Gd (**4**) and Eu (**5**)), $[LnL_2(tmh)(CH_3OH)]\cdot n\ H_2O\cdot m\ CH_3OH$ (Ln^{III} = Yb (**1b**), Er (**2b**), Dy (**3b**), Gd (**4b**)) and $[LnL_2(tta)(CH_3OH)]\cdot CH_3OH$ (Ln^{III} = Yb (**1c**), Er (**2c**), Dy (**3c**), Gd (**4c**) have been prepared from the reaction of $Ln(CF_3SO_3)\cdot nH_2O$ salts with the tridentate ligand 2-(tetrazolate-5-yl)-1,10-phenanthroline (HL). For the two latter sets, additionally with the respective β-diketonate ligands 2,2,6,6-tetramethylheptanoate (tmh) or 2-thenoyltrifluoroacetonate (tta). In the $[LnL_3]\cdot CH_3OH$ complexes the Ln^{III} ions are coordinated to three phenanthroline-tetrazolate ligands showing a LnN_9 coordination sphere. Dynamic *ac* magnetic measurements for **1** – **3** reveal that these complexes only exhibit single molecule magnet (SMM) behaviour when an external *dc* magnetic field is applied, with U_{eff} values of 11.7 K (**1**), 16.0 K (**2**) and 20.2 K (**3**). When the tridentate phenanthroline-tetrazolate ligand is replaced by one molecule of methanol and the *β*-diketonate ligand tmh (**1b – 3b**) or tta (**1c – 3c**), a significant increase in U_{eff} occurs and, in the case of the Dy^{III} derivates **3b** and **3c**, out-of-phase χ'' signals below 15 K and 10 K, respectively, are observed under zero-*dc* magnetic field. CASSCF+RASSI ab initio calculations performed on the Dy^{III} derivates support the experimental results. Thus, for **3** the ground Kramers' doublet is far from being axial and the first excited state is found to be very

close in energy to the ground state so the relaxation barrier in this case is almost negligible. Conversely, for **3b** and **3c**, the ground Kramers' doublet is axial with a small quantum tunneling of the magnetization (QTM) and the energy difference between the ground and first Kramers' doublets is much higher, which allows these compounds to behave as SMMs at zero-field. Moreover, these calculations support the larger U_{eff} observed for **3b** compared to **3c**. Additionally, the solid-state photophysical properties of **1**, **2**, **4** and **5** show that the phenanthroline tetrazolate ligand can act as an effective antenna to sensitize the characteristic Yb^{III}, Er^{III} and Eu^{III} emissions through an energy transfer process.

INTRODUCTION

Tetrazole ligands have been widely used in the last few decades to prepare plentiful *n*d-transition metal complexes (*n* = 3, 4, 5) with interest in fields such as molecular magnetism, MOFs or photochemistry, among others.[1-6] 5-substituted tetrazoles show several intrinsic properties that make them very attractive from the point of view of coordination chemistry: *i)* first of all, they are very easy to prepare. Since the first practical procedure described by Finnegan[2] involving the reaction of nitriles and sodium azide in the presence of ammonium chloride, several synthetic protocols have been established allowing for the preparation of these ligands with a vast range of 5-substituents in excellent yields under mild synthetic conditions and short reaction times;[3] *ii)* when deprotonated, they form strongly basic tetrazolate anions that are able to coordinate transition metal cations through a wide variety of coordination modes;[4] *iii)* additionally, the tetrazolate ring is highly reactive towards electrophilic agents allowing for their functionalization with several functional groups such as amines or carboxylic acids.[5] Regarding the 4f-block of elements, several Eu^{III}- and Tb^{III}-tetrazolate complexes with remarkable luminescent properties have also been recently reported.[6] The structural and stability properties of some lanthanide tetrazolate complexes have been found to be similar to those of the carboxylate analogous,[6a,b] although the replacement of the carboxylate group with tetrazolate induces a significant red-shift of the lowest-energy absorption bands in the UV-Vis spectra, allowing for the luminescence of these complexes to be effectively sensitized with visible light. Surprisingly, to the best of our knowledge no examples of $Dy^{III,}$ $Er^{III,}$ or Yb^{III} complexes with tetrazole-based ligands have been reported thus far. Compared to Eu^{III}, these lanthanides also display interesting luminescence properties in the visible or near-infrared spectroscopic regions[7] as well as

exciting magnetic properties.[8] They have particularly stimulated the research activity in the field of Molecular Magnetism due to their ability to behave as single-molecule magnets (SMMs). These systems are molecular complexes exhibiting slow relaxation of the magnetization and magnetic hysteresis below a certain temperature, known as blocking temperature (T_B).[8,9] It is worth noting that these nanomagnets present potentially outstanding future applications in fields such as molecular spintronics,[10] ultra-high density magnetic information storage[10,11] and as qubits for quantum computing at the molecular level.[12] The SMM behavior arises essentially from the existence of an anisotropic energy barrier (U) that prevents magnetization reversal below T_B when the magnetic polarizing field is removed.[9a] The utility of the lanthanide ions in this field is due to the fact that they exhibit strong magnetic anisotropy due to the combination of strong spin-orbit coupling and crystal-field effects promoted by the ligand surrounding.[8] In fact numerous 3d/4f and 4f (and 5f) mononuclear and polynuclear coordination compounds, most of them containing Dy^{III} ions,[8,9,13] have been reported to exhibit SMM behavior, which is usually due to the individual Ln^{III} ions and their coordination sphere, rather than to the whole molecule. Interestingly, mononuclear 4f metal complexes have been shown to possess energy barriers an order of magnitude higher than observed in 3d and 3d/4f polymetallic clusters. SMM are generally constructed by assembling lanthanide ions with inorganic or organic ligands containing either only oxygen donor atoms or a combination of oxygen and nitrogen donor atoms or only nitrogen donor atoms (organometallic complexes containing only carbon[14] donor atoms with or without nitrogen,[15] sulphur[16], phosphorous, arsenic or selenium[17], bridging groups are less abundant). Some typical examples of Dy-SMMs containing a combination of oxygen and nitrogen donor atoms compounds are Dy(diimine)(tris(β-diketonate) complexes (diimine = bipyridine, phenanthroline, bipyrimidine), some which exhibit large anisotropic energy barriers for the reversal of the magnetization.[18] As far as we know, no examples of SMMs containing either only tetrazolate ligands or tetrazolate/β-diketonate mixed ligands have been reported so far.

Here, we report on the synthesis, structure, magnetic and luminescent properties of three sets of mononuclear 4f-complexes prepared from the tridentate ligand 2-(tetrazolate-5-yl)-1,10-phenanthroline (HL, scheme 1). For the first set, the lanthanide ions (Ln^{III} = Yb, Er and Dy) are coordinated to three L^- ligands, showing a LnN_9 coordination sphere. It is worth mentioning that examples of non-phthalocyaninate Dy-containing SMMs (induced by the magnetic field) in

which the Dy^{III} ion are surrounded exclusively by nitrogen donor atoms are very scarce.[19] For the second and third sets, the coordination sphere around the Ln^{III} ions is of the type LnN_6O_3, where a phenanthroline-tetrazolate ligand has been replaced by one molecule of methanol and the β-diketonate ligands 2,2,6,6-tetramethylheptane-3,5-dionate (tmh) or 2-thenoyltrifluoroacetonate (tta). The aim of this work is two-fold: (i) to know whether or not the LnN_9 complexes exhibit SMM properties and to analyze how these properties vary when the L^- ligand is substituted by different β-diketonate ligands and (ii) to elucidate if the ligand L^- in isolation acts as an effective sensitizer for red (Ln^{III} = Eu) and NIR (Ln^{III} = Nd, Er, Yb) luminescence. If SMM and luminescence properties coexist in these complexes, these new systems represent bifunctional luminescent-SMMs mononuclear complexes.

EXPERIMENTAL SECTION

General procedures

Unless stated otherwise, all reactions were conducted in oven-dried glassware in aerobic conditions. Reagents and solvents purchased from commercial sources were used as received. The ligand 2-(2*H*-tetrazol-5-yl)-1,10-phenanthroline (HL) was prepared as previously reported by Gao et *al*.[20]

Preparation of complexes

*$[Ln(L)_3]\cdot CH_3OH$ [Ln^{III} = Yb (**1**), Er (**2**), Dy (**3**), Gd (**4**), Eu (**5**)]*. A general procedure was followed for the synthesis of these complexes. 0.15 mmol of the appropriate $Ln(CF_3SO_3)\cdot nH_2O$ dissolved in methanol (10 mL) was added without stirring to a mixture containing three equivalents of HL ligand (0.45 mmol, 110 mg) and the stoichiometric amount of triethylamine in methanol (20 mL). The resulting yellow solutions were allowed to stand at room temperature. Slow evaporation of the solvent over a period of 1 – 2 days afforded for complexes **1** – **5** as a good crop of single crystals suitable for X-ray diffraction which were filtered, washed with a minimum amount of methanol and air-dried.

*$[Ln(L)_2(tmh)(CH_3OH)]\cdot mCH_3OH\cdot nH_2O$ [Ln^{III} = Yb (**1b**), Er (**2b**), Dy (**3b**), Gd (**4b**)]*. Following a similar procedure, 0.015 mmol of $Ln(CH_3SO_3)_3\cdot nH_2O$

dissolved in CH_3OH (20 mL) was added without stirring to a solution containing 0.015 mmol of Htmh (2,2,6,6-tetramethylheptane-3,5-dione), 0.030 mmol of HL and 0.045 mmol of triethylamine in 20 mL of CH_3OH. After a few hours, well-formed crystals were obtained in good yield. The crystals were stable while submerged in their mother liquor. A severe and rapid crystalline degradation was observed when the crystals were isolated and dried.

*$[Ln(L)_2(tta)(CH_3OH)]\cdot CH_3OH$ [Ln^{III} = Yb (**1c**), Er (**2c**), Dy (**3c**), Gd (**4c**),]*. These complexes were prepared as the *tmh* derivates, but using 2-thenoyltrifluoroacetone (H*tta*) instead.

Elemental analyses for these compounds are given in the ESI (Table S1).

Physical Measurements

Elemental analyses were carried out at the "Centro de Instrumentación Científica" of the University of Granada on a Fisons-Carlo Erba analyser model EA 1108. IR spectra on powdered samples were recorded with a ThermoNicolet IR200FTIR using KBr pellets. Alternating current susceptibility measurements under different applied static fields were performed using an oscillating ac field of 3.5 Oe and ac frequencies ranging from 1 to 1500 Hz with a Quantum Design SQUID MPMS XL-5 device. Ac magnetic susceptibility measurements in the range 1 – 10000 Hz were carried out with a Quantum Design Physical Property Measurement System using an oscillating ac field of 5 Oe. UV-Vis spectra were measured on a UV-1800 Shimadzu spectrophotometer and the photoluminescence spectra on a Varian Cary Eclipse spectrofluorometer. Lifetime data were obtained on a JobinYvon-Horiba Fluorolog spectrometer fitted with a JY TBX picoseconds photodetection module. All near-IR photophysical data were obtained on a JobinYvon-Horiba Fluorolog-3 spectrometer fitted with a Hamamatsu R5509-73 detector (cooled to -89 ºC using a C9940 housing). For the near-IR lifetimes the pulsed laser source was a Continuum MiniliteNd:YAG configured for 355 nm output. Luminescence lifetime profiles were obtained using the JobinYvon-Horiba FluoroHub single photon counting module, and the data fits yielded the lifetime values using the provided DAS6 deconvolution software. X-Ray Powder diffraction patterns were

collected using a high-throughput Bruker D8 Advance diffractometer working on transmission mode and equipped with a focusing Göbel mirror producing CuKα radiation (λ = 1.5418 Å) and a LYNXEYE detector. Data were collected at room temperature (RT), in the 2θ range 3 to 35˚, with a 0.02˚ step width.

Single-Crystal Structure Determination

Suitable crystals of the different complexes were mounted on a glass fiber and used for data collection at 100(2) K. Data for **1**, **3**, **5**, **1b - 3b** and were collected with a Bruker AXS APEX CCD area detector equipped with graphite monochromated Mo Kα radiation (λ = 0.71073 Å) by applying the ω-scan method. Data for **2 - 4** and **1c – 4c** were collected with a Bruker D8 Venture (Mo Kα radiation, λ = 0.71073 Å, Photon 100 CMOS detector). Using Olex2[21], the structures were solved by either Patterson or direct methods with SHELXS and refined with full-matrix least-squares calculations on F^2 using SHELXL[22]. Lorentz-polarization and empirical absorption corrections were applied. Anisotropic temperature factors were assigned to all atoms except for the hydrogens, which are riding their parent atoms with an isotropic temperature factor arbitrarily chosen as 1.2 times that of the respective parent. Final *R(F)*, $wR(F^2)$, goodness of fit agreement factors, and details of the data collection and analysis can be found in Supporting Information (Tables S2-S4). Selected bond lengths and angles are given in Supporting Information (Tables S5-S10). The X-ray studies for **1b - 4b** were carried out with the samples embedded in oil in order to preserve their crystallinity. In the case of **4b**, the hydrogen atoms associated to the disordered methanol molecule C3S(B)-O3S could not be located from difference Fourier maps.

Computational Details:

Low-energy spectra and g factors of the eight lowest Kramers' doublets of **1** were obtained by means of CASSCF+RASSI calculations, as implemented in the MOLCAS 8.0 software package.[23] The method is divided into two steps: (i) CASSCF(9,7) calculations for three different multiplicities (sextet, quartet and doublet) (ii) The effect of spin-orbit coupling on the basis of the converged wavefunctions obtained in the previous step is included by the Restricted Active Space State Interaction (RASSI) method. Spin Hamiltonian parameters (such as g factors) can be calculated from the

wavefunctions resulting after the state interaction step employing the SINGLE_ANISO program.[24] We included 21, 128 and 98 roots for the sextet, quartet and doublet Dy^{III} CASSCF calculations, while for the Er^{III} systems 35 and 112 quartets and doublet states, respectively were employed and 7 doublet states for the Yb^{III} calculations. The employed basis set has the following contractions: Dy, Er, Yb[9s8p6d4f3g2h]; S 4s3p1d, F 4s3p2d1f; O [4s3p2d1f]; N [4s3p2d1f]; C [3s2p]; H [2s]. The structure of the model was extracted from the corresponding X-ray structure without any ligand truncation. Electrostatic potential maps were obtained by DFT calculations (functional: B3LYP basis,[25] TZVP program,[26] Gaussian09[27]) employing the geometry for the ligand environment of the previous CASSCF+RASSI calculations and removing the Dy^{III} ion.

RESULTS AND DISCUSSION

Synthesis and structural characterization of $[LnL_3]\cdot CH_3OH$ (1 – 5), $[LnL_2(tmh)(CH_3OH)]$ (1b – 4b) and $[LnL_2(tta)(CH_3OH)]$ (1c – 4c) complexes.

Complexes **1 - 5** were synthesized by mixing $Ln(CF_3SO_3)_3\cdot n\ H_2O$ with HL and triethylamine in methanol without stirring using a 1:3:3 molar ratio (see scheme 1). Complexes **1b - 4b** and **1c – 4c** were prepared following a similar procedure by mixing the Ln^{III} trifluoromethanesulfonate with HL, Htmh (2,2,6,6-tetramethylheptane-3,5-dione) or Htta (2-thenoyltrifluoroacetone) and Et_3N in a 1:2:1:3 molar ratio (see scheme 1).

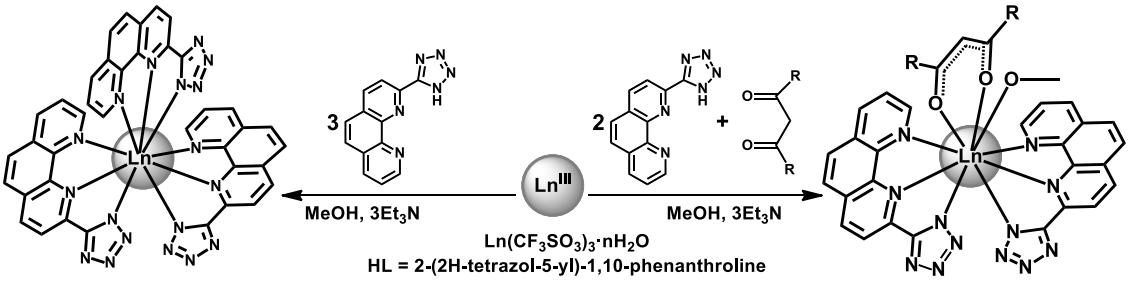

Scheme 1.- Reactivity of the HL ligand and complexes prepared in this work.

X-Ray crystallographic studies revealed that **1** – **5** are isostructural compounds crystallizing in the monoclinic space group $P2_1/c$. In general, the structures consist of mononuclear $[LnL_3]$ entities and one crystallization molecule

of methanol. Within the mononuclear units, the lanthanide ions are coordinated by three deprotonated phenanthroline-tetrazolate ligands disposed in an "up – up – down" arrangement around the lanthanide resulting in a C_1 symmetry of the complex. The LnN_9 coordination environment is comprised of three N atoms of the tetrazolate (N_{tz}) rings (N6, N12 and N18) and six N atoms of the three phenanthroline (N_{ph}) moieties (N1, N2, N7, N8, N13 and N14). According to the continuous-shape-measures (CShMs) method,[28] the lowest shape measures for the LnN_9 coordination belong to a C_{4v} spherical capped square antiprism (CSAPR) geometry in the range 0.932 (**1**) – 1.194 (**5**) (Table S11). As expected, the Ln – N bond lengths decrease from Eu^{III} to Yb^{III} due to lanthanide contraction. The decrease of ionic radii along the series also affects the planarity of the coordinated ligands. Whereas for the Eu^{III} derivate (**5**) the torsion angles between the phenanthroline and tetrazolate rings are within the range 0.75º – 4.82º, for the Yb^{III} derivate (**1**) the range increase to 3.44º - 11.03º probably due to steric hindrance. The Ln-N_{tz} bond distances are significantly shorter than those observed for the Ln-N_{ph} bonds which points out the strength of the electrostatic interaction between the metal cation and the anionic tetrazolate ring.

Complexes **1b – 4b** are also isostructural and crystallize in the triclinic P-1 space group. The structures consist of mononuclear $[Ln(L)_2(tmh)(CH_3OH)]$ entities and molecules of methanol and water of crystallization. The Ln^{III} ion exhibits a LnN_6O_3 coordination sphere with the lowest shape measures for the C_{4v} CSAPR geometry in the range 0.694 (**2b**) - 1.063 (**4b**) (Table S11). As observed previously for **1 – 5**, the two Ln-N_{ttz} bond distances are short compared to the Ln-N_{ph} bonds. They are, however, significantly longer than those of the Ln-O_{tmh} bonds. The electrostatic interaction between the Ln^{III} center and the β-diketonate ligands is stronger than that showed by the tetrazolate anions. As expected, the Ln-N and Ln-O bond distances decrease as the atomic number of the Ln^{III} center increases. The nitrogen atoms of the tetrazolate groups in L^- are connected with solvated methanol and/or water molecules along the crystalline network through strong hydrogen-bond interactions.

The main structural features of complexes **1c – 4c** are very similar to those observed for **1b – 4b**. All the complexes are isostructural and crystallize in the P-1 spatial group of symmetry. The lowest shape measures for the LnN_6O_3 coordination sphere belong also to C_{4v} CSAPR geometry and are found in the

range 0.730 (**1c**) – 0.834 (**4c**)). The atomic distances around the Ln^{III} unit follows the expected trend Ln-N_{phen}>Ln-N_{ttz}>>Ln-O_{tta} and a slight steric crowding is observed as the atomic number of the lanthanide ion increases and, therefore, its size decreases. In this set of complexes, the unit cell contains a crystallization molecule of methanol involved in a strong H-bond interaction with a nitrogen atom of one of the tetrazolate ring.

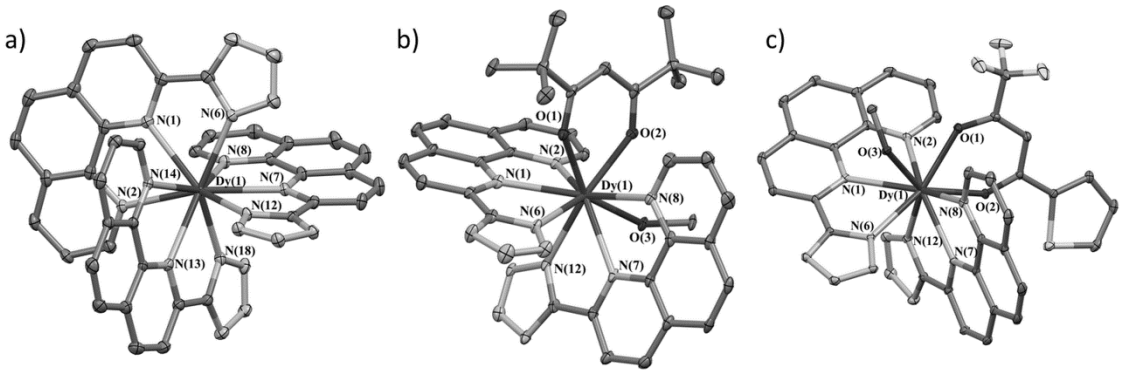

Figure 1.- Crystal structures of complexes **3** (a), **3b** (b) and **3c** (c). Lattice solvents molecules and hydrogen atoms have been omitted for the sake of clarity. Ellipsoids are drawn at 50 % probability.

Magnetic properties

The direct-current (*dc*) magnetic susceptibilities (χ_M) of complexes **1-4**, **1b-4b** and **1c-4c** have been measured in the 2-300 K temperature range under an applied magnetic field of 0.1 T and are shown in Figure S1 in the form $\chi_M T$ *vs* T.

The room temperature $\chi_M T$ values for all the complexes are very close to those calculated for isolated Ln^{III} ions in the free-ion approximation (see Table 1).

Table 1: Direct current magnetic data for the complexes studied in this work.

Ground state of the Ln^{III} ion	**Theoretical $\chi_M T$ value (cm^3 K mol^{-1})[a]**	**Theoretical M_{sat} value ($N\mu_B$)[b]**	**Compound**	**Experimental $\chi_M T_{300K}$ / $\chi_M T_{2K}$ (cm^3 K mol^{-1})**	**Experimental M_{sat} value (T =2 K, H = 5 T) ($N\mu_B$)**
Yb^{III}	2.57	4	**1**	2.21 / 1.99	1.94
$^2F_{7/2}$, g_J =8/7			**1b**	2.24 / 1.44	1.74
			1c	2.25 / 1.48	1.83
Er^{III}	11.48	9	**2**	10.38 / 7.34	5.35
$^4I_{15/2}$, g_J =6/5			**2b**	13.04 / 5.7	4.23

			2c	11.29 / 5.39	5.29
Dy^{III}	14.17	10	**3**	13.38 / 9.37	5.60
$^6H_{15/2}$, g_J =4/3			**3b**	15.52 / 12.60	5.61
			3c	14.02 / 10.40	4.98
Gd^{III}	7.875	7	**4**	7.65 / 7.55	6.72
$^8S_{7/2}$, g_J =2			**4b**	8.37/7.93	7.24
			4c	7.34 / 7.00	6.93

[a] $\chi_M T = \frac{N\beta^2}{3k}\{g_J^2 J(J+1)\}$ [b] $M = NJ\mu_B;\ J = L + S\ ;\ g_J = \frac{3}{2} + \frac{S_T(S_T+1) - L(L+1)}{2J(J+1)}$

On cooling, the $\chi_M T$ product of the complexes **1-3**, **1b-3b** and **1c-3c** steadily decreases down to 2 K, which is due to the depopulation of the excited m_j sublevels of the Ln^{III} ions, which arise from the splitting of the spin-orbit ground terms ($^2F_{7/2}$, $^4I_{15/2}$ and $^6H_{15/2}$, for Yb^{III}, Er^{III} and Dy^{III}, respectively), by the ligand field, and/or possible very weak intermolecular interactions between the Ln^{III} ions. The $\chi_M T$ product for the Gd^{III} compounds (**4, 4b** and **4c**) remains almost constant from room temperature to 2 K, as expected for such an isotropic ion.

The field dependence of the magnetization for complexes **1-3**, **1b-3b** and **1c-3c** are given in Figure S2. The *M* versus *H* plot at 2 K for these complexes shows a relatively rapid increase in the magnetization at low field to reach almost saturation for magnetic fields of 5T. The observed saturation values for these complexes (see Table 1) are rather lower than the calculated ones, which is due to crystal-field effects leading to significant magnetic anisotropy.[29] The field dependence of the magnetization at 2 K for the compounds **4**, **4b** and **4c** follows the Brillouin function for a S =7/2 systems, as expected.

Single Molecule Magnet behavior.

In order to know if the complexes **1-3**, **1b-3b** and **1c-3c** behave as mononuclear single-molecule magnets, dynamic *ac* magnetic susceptibility measurements as a function of the temperature and frequency were performed on these samples. Under a zero-external dc field, none of the ytterbium complexes (**1**, **1b** and **1c**) exhibited out-of-phase (χ''_M) signals. This behavior can be attributed either to the fact that the energy barrier for the flipping of the

magnetization is too small to trap the magnetization in one of the equivalent configurations above 2 *K*, or to the fast relaxation of the magnetization through quantum tunnelling (QTM). When the *ac* measurements were performed in the presence of an external *dc* field of 1000 G to fully or partly suppress the QTM, complexes **1**, **1b** and **1c** showed frequency dependence of the out-of-phase (χ''_M) signals typical of thermally activated relaxation processes and SMM behavior (Figure 2 and Figures S3 – S5), with out-of-phase χ''_M peaks in the ranges 3.5 K (1400 Hz) – 2.5 K (300 Hz), 5.0 K (1400 Hz) – 3 K (300 Hz) and 4.75 K (1400 Hz) – 2.5 K (80 Hz), respectively. In the cases of complexes **1** and **1c**, the out-of-phase susceptibility tends to zero after the maxima which indicates that the quantum tunnelling of the magnetization has been effectively suppressed. For **1b** the out-of-phase susceptibility increases slightly below 2 K at low frequencies thus indicating that the QTM relaxation process has not been fully cancelled in this complex. The values of the energy barriers for the reversal of the magnetization (U_{eff}) and the relaxation times (τ_o) were extracted from the fit of the frequency dependence of χ''_M at each temperature to the Debye model (Figures S4 in Supporting Information) and are reported in Table 1. Virtually identical values were obtained for U_{eff} and τ_o by fitting the frequencies of the maxima ($\tau = 1/2\pi f$) observed for the χ''_M signals and the temperatures to an Arrhenius plot.

It should be noted that Raman relaxation processes are usually proposed for Yb^{III} complexes.[30] In view of this we decided to fit the experimental data also to an equation that considers that the spin-lattice relaxation takes place through a Raman process ($\tau^{-1} = BT^n$) . In general n = 9 for Kramers' ions such as Yb^{III},[31] but depending on the structure of the levels, n values between 1 and 6 can be considered as reasonable.[32] The fit of the experimental data is excellent, which could indicate that the spin-lattice relaxation is not of the thermally activated type, but takes place through an optical acoustic Raman-like process.

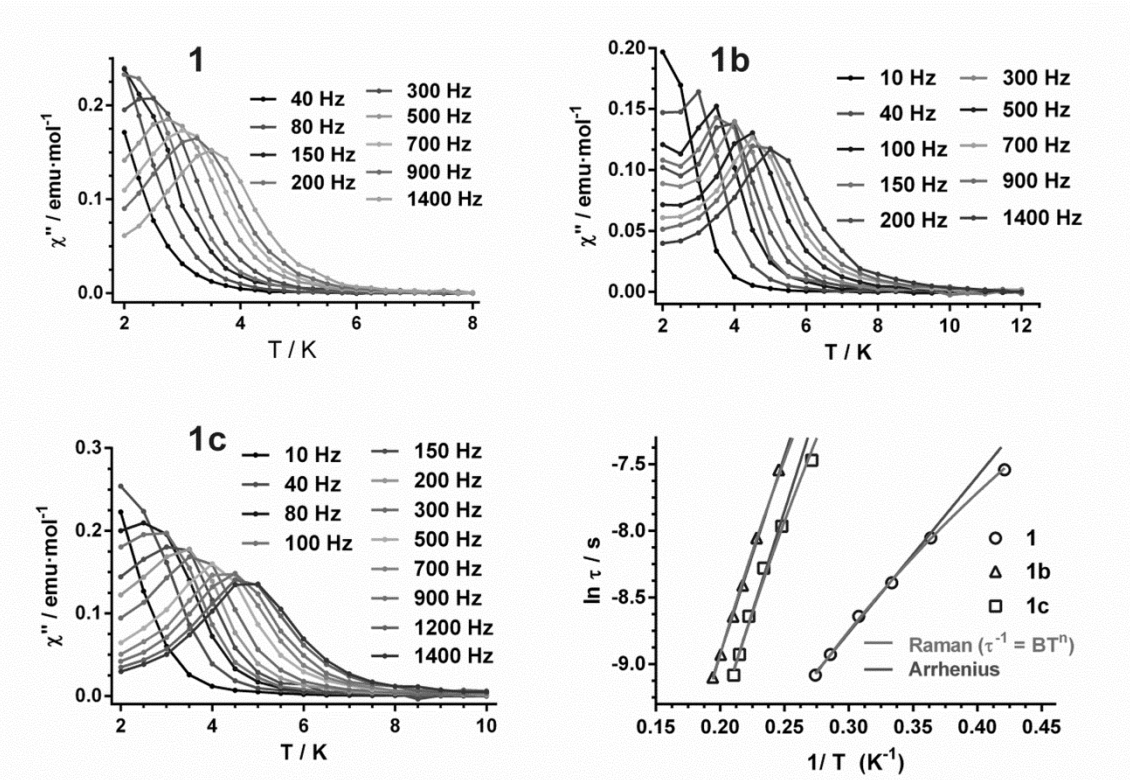

Figure 2.- Temperature dependence of in-phase out-of-phase χ''_M component of the *ac* susceptibility for Yb^{III} complexes **1** (top left), **1b** (top right) and **1c** (bottom left) under an applied *dc* field of 1000 Oe (the solid lines are guides to the eye). Arrhenius (red lines) and Raman (green lines) plots of relaxation times (bottom right). The solid lines represent the best fitting of the experimental data for **1**, **1b** and **1c** to the Arrhenius equation for a thermally activated process or to a Raman relaxation process.

Table 2.- U_{eff} and τ_o values for the reported complexes.

Complex	Orbach (H_{dc} =1000 Oe)		Raman ($\tau^{-1} = BT^n$)		Raman + Orbach			
	U_{eff} (K)	τ_o (s)	B	n	B	n	U_{eff} (K)	τ_o (s)
1	11.7	$4.6\cdot10^{-6}$	82.1	3.6				
1b	29.7	$3.5\cdot10^{-7}$	0.2	6.5				
1c	30.3	$2.0\cdot10^{-7}$	0.3	6.5				
2	16.0[a]	$5.3\cdot10^{-8}$						
2b	30.4	$7.8\cdot10^{-8}$			4.1	5.2	49.2	$3.8\cdot10^{-9}$
2c	25.8[a]	$3.5\cdot10^{-8}$						
3[b]	13.7	$1.2\cdot10^{-7}$			$1.2\cdot10^{-6}$	9.0	20.2	$2.1\cdot10^{-8}$
3b	95.7	$3.4\cdot10^{-7}$			0.002	5.5	170.1	$1.2\cdot10^{-9}$
3c	76.0	$4.2\cdot10^{-8}$			0.003	6.4	136.1	$1.2\cdot10^{-10}$

[a] Calculated with the equation $\ln(\chi''_M/\chi'_M) = \ln(\omega\tau_0)-U_{eff}/kT$. [b] In this complex, competing Raman, Orbach and direct relaxation processes were considered ($\tau^{-1} = AT + BT^n + \tau_0^{-1} exp(-U_{eff}/k_BT)$ with A = 9.4 and n fixed at n = 9).

The replacement of L^- by a β-diketone bidentate ligand in the YbN_9 coordination sphere of **1** to afford a YbN_6O_3 coordination environment in **1b** and **1c** seems to provoke a significant increase of the thermal energy barrier (in the case of a thermally activated relaxation process) or in the energy gap between the ground state and a virtual state (in the case of a Raman relaxation process).

The Cole-Cole plots (Figure S5) for **1**, **1b** and **1c** show, in the temperature regions where appear the maxima in the χ''_M vs T plots, semi-circular shapes with α values (this parameter determines the width of the distribution of relaxation times, so that α = 1 corresponds to an infinitely wide distribution of relaxation times, whereas α = 0 describes a single relaxation process) in the 0.096-0.013, 0.17-0.06 and 0.2-0.017 ranges, respectively, thus indicating the presence of a very narrow distribution of slow relaxation processes in those regions.

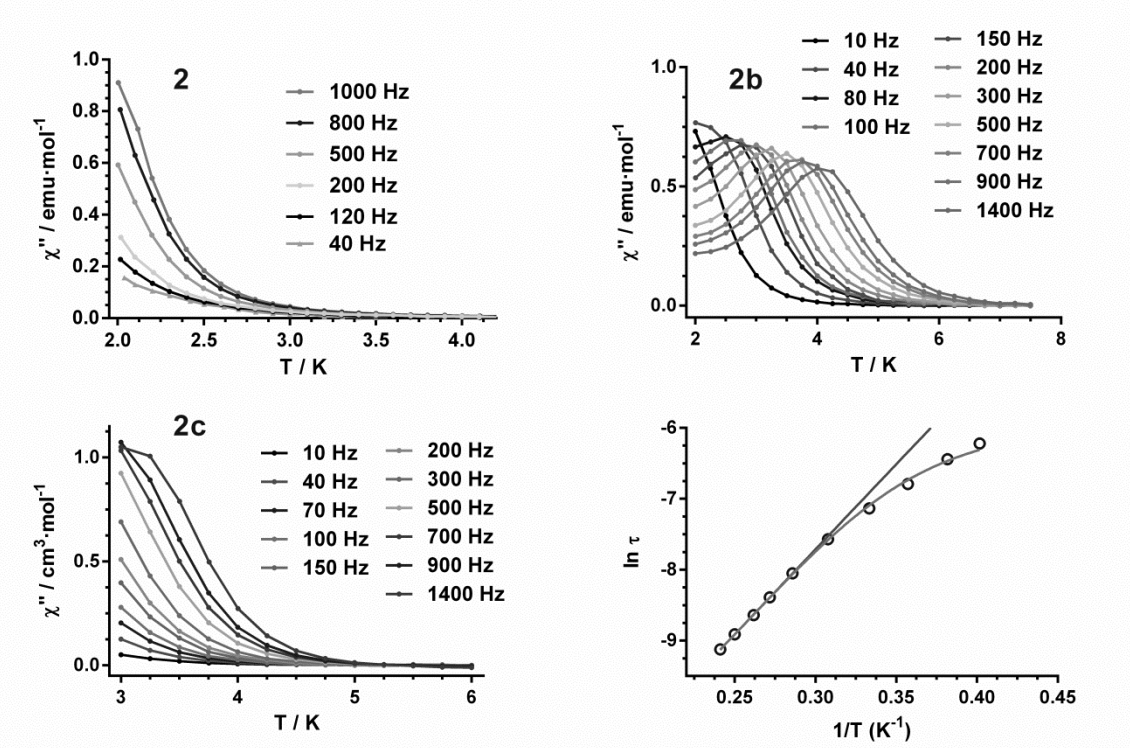

Figure 3.- Temperature dependence of in-phase out-of-phase χ''_M component of the *ac* susceptibility for Er^{III} complexes **2** (top left), **2b** (top right) and **2c** (bottom left) under a applied *dc* field of 1000 Oe (the solid lines are guides to the eye). Arrhenius (red lines) and Raman (green lines) plots of relaxation times for **2b** (bottom right). The solid lines represent the best fit of the experimental data to the Arrhenius equation for a thermally activated process or to a Raman relaxation process.

The erbium complexes **2a–2c** do not show out-of-phase ac signals at zero *dc* applied field, which, as in the complexes **1a–1c**, could be due to the existence of a very small thermal energy barrier for the reversal of the magnetization as to block the magnetization above 2 *K* and/or the occurrence of a fast QTM relaxation process. In the presence of a field of 1000 Oe, to fully or partly annul the possible QTM, the compounds **2** and **2c** show slow relaxation of the magnetization without maxima above 2 K. Nevertheless, the χ''_M signals appear at higher temperatures in **2c** than in **2**. The χ''_M *vs* T plot for **2b**, however, displays the frequency dependence of χ''_M in the temperature range 4 K (1400 Hz)-2.5 K (80 Hz), which points to the existence of SMM behaviour induced by the *dc* magnetic field. The relaxation times extracted from the frequency-dependent

susceptibility data follow an Arrhenius law with an effective energy barrier for the reversal of the magnetization U_{eff} = 30.4 K and $\tau_o = 7.7 \cdot 10^{-8}$ s (Figure 3, bottom right). The Cole-Cole diagram for **2b** in the temperature range 4.25 - 2.25 K (Figure S8) exhibits semicircular shapes and can be fitted using the generalized Debye model, affording α values in the range 0.043(4.25 K) - 0.37(2.25 K), which suggest the existence of more than one relaxation process. In view of this, we have fitted the temperature dependence of the relaxation times to a combination of thermally activated (Orbach) and Raman processes. The extracted values are given in Table 1. In order to make a quantitative comparison with **2b**, the Debye equation $\ln(\chi''_M/\chi'_M) = \ln(\omega\tau_0)-U_{eff}/kT$ was used to calculate τ_0 and U_{eff} for **2** and **2c** (Figure S9 and Table 1). As in the case of the ytterbium complexes, the energy barrier dramatically increases on passing from **2** to **2b** and **2c**.

Ac magnetic susceptibility measurements as a function of the temperature and frequency under zero and 1000 Oe *dc* fields for compounds **3**, **3b** and **3c** show that only the two latter compounds display frequency dependence for the out-of-phase (χ''_M) signals below 15 K and 10 K, respectively, typical of thermally activated relaxation processes at zero-field (Figure S11). However, no neat maxima appear in the temperature dependence of the out-of-phase (χ''_M) signals at different frequencies, which could be due to overlapping of different relaxation processes, including a faster QTM relaxation process even at frequencies as high as 1400 Hz. This behaviour seems to indicate that **3b** and **3c** present slow relaxation of the magnetization and SMM behaviour at zero dc applied field. The increase of the out-of-phase (χ''_M) signals at very low temperature is an unambiguous indication of the existence of fast QTM.

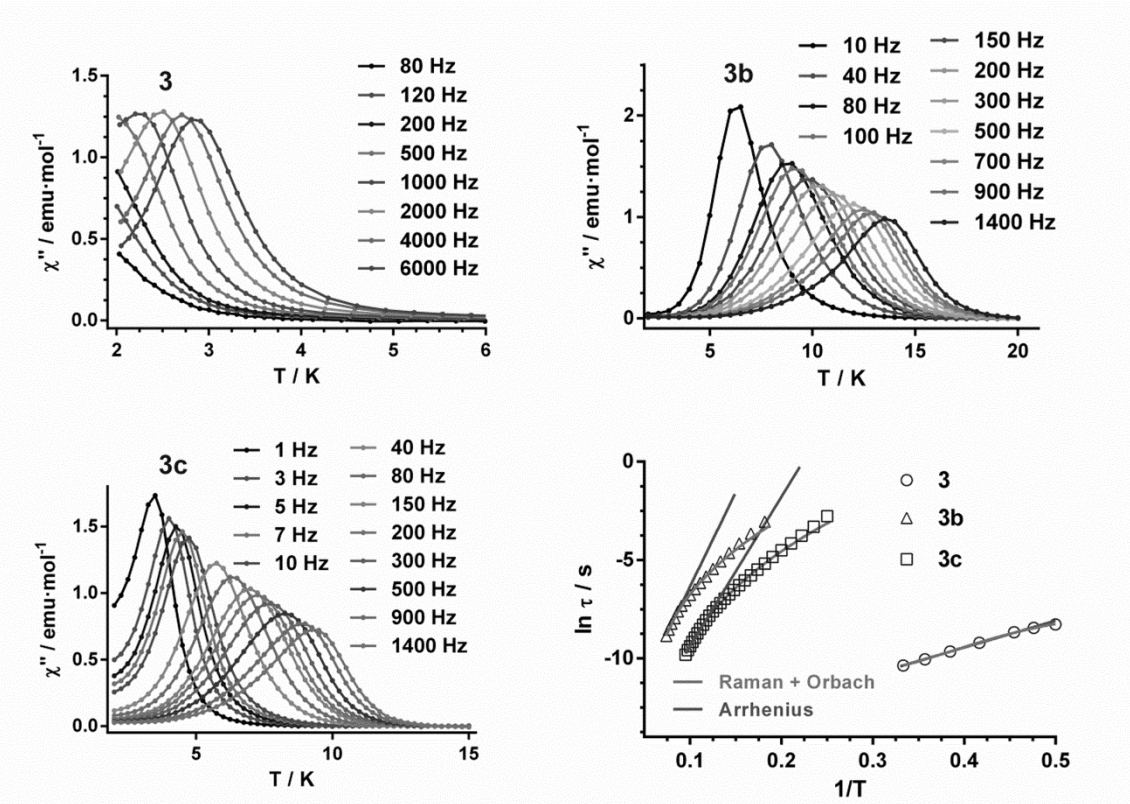

Figure 4.- Temperature dependence of in-phase out-of-phase χ''_M component of the *ac* susceptibility for Dy^{III} complexes **3** (top left), **3b** (top right) and **3c** (bottom left) under a applied *dc* field of 1000 Oe (the solid lines are guides to the eye). Arrhenius (red lines) and Raman (green lines) plots of relaxation times (bottom right). The solid lines represent the best fitting of the experimental data for **3**, **3b** and **3c** to the Arrhenius equation for a thermally activated process or to a Raman relaxation process.

When the *ac* measurements were performed in the presence of a small external *dc* field (Figure 4) of 1000 Oe to completely or partially suppress the fast QTM relaxation process, the tails at low temperatures disappeared, giving rise to well defined out-of-phase susceptibility peaks in the temperature ranges 2.8 K (6000 Hz)-2.20 K (80 Hz), 13.5 K (1400 Hz)-6 K (10 Hz), 9.3 K (1400 Hz)-3.5 K (10 Hz). The Cole-Cole diagram for these complexes (Figure S13) exhibit semicircular shapes and can be fitted using the generalized Debye model, affording α values in the ranges 0.2 (2.2 K)-0.1(3.0 K), 0.06 (6.0 K)-0.006 (14.0 K), 0.24 (4.0 K)-0.04 (9.0 K), which clearly suggest the existence of more than one relaxation process in compounds **3** and **3c**. The frequency dependence of χ''_M at each temperature was fitted to the generalized Debye model (Figure S12), which

allowed the relaxation times, τ, to be extracted. The fitting of τ to the Arrhenius law afforded the effective energy barriers for the reversal of the magnetization listed in Table 1. The fact that the data deviate from linearity in the low temperature region, suggests the existence of competing Raman and Orbach processes and therefore, we have fitted the experimental data to the following equation, which includes contributions of both relaxation processes:

$$\tau^{-1} = BT^{n} + \tau_0^{-1} \exp(-U_{eff}/k_BT) \qquad (1)$$

The best fit of the experimental data afforded higher effective energy barriers for the reversal of magnetization and lower flipping rates than the simple Arrehnius law, which are indicated in Table 1 together with other significant parameters.

It is worth mentioning that no obvious hysteresis loop can be observed at 2.0 K, even for the Dy^{III} complexes, which could be due to the QTM and the slow magnetic field variation speed of our conventional SQUID.

It is well known that mononuclear Dy^{III} complexes often exhibit SMM behaviour as they show an $M_j = \pm 15/2$ Kramers' doublet ground state with axial anisotropy.[8b,9a]. We have performed electronic structure calculations based on CASSCF methods[23] to estimate the values of the thermal energy barrier and to gain insight into the mechanism of the slow magnetic relaxation. From the nine complexes studied (**1-3**, **1b-3b** and **1c-3c**, see Table 3), only two of them, **3b** and **3c**, show slow relaxation of the magnetization at zero dc field. This type of calculations allows for the estimation of excitation energies, spin-Hamiltonian parameters (Landé g-factors) and relaxation pathways for the lanthanide complexes. From the analysis of calculated spin-Hamiltonian parameters (see Table 3), we observe strong axial anisotropy for **3b** and **3c**, in agreement with the observed zero-field SMM properties of these compounds. It is worth noting that all the remaining complexes (all the three Yb^{3+} and Er^{3+} derivatives and the Dy^{3+} derivative **3**) present markedly higher deviations from purely axial anisotropy, as evidenced by their larger values of g_x and g_y in comparison to **3b** and **3c.**

From the CASSCF-RASSI excitation energies (Table 3) we can observe that complex **3** presents, after the inclusion of spin-orbit effects, a very low first excited state (SO-E1), which severely limits the existence of a pronounced relaxation barrier for this compound. On the other hand, the excitation energies between the ground and second

Kramers' doublets (KD) for **3b** and **3c** are comparable with other Dy compounds that behave as SMMs.[8,9] The calculated U_{eff} values (energy gap between the ground and first excited KDs) follow the same trend as the experimental ones but are almost 50 % larger. However, when Orbach and Raman relaxation processes are considered to occur simultaneously, the experimental U_{eff} values are more comparable, but still lower than the calculated ones. The difference between the experimental and calculated U_{eff} values could be due to limitations inherent to the CASSCF method.[33] In fact the calculated U_{eff} values are usually overestimated, probably due to the existence of spin relaxation mechanism between neighbour molecules that are not considered in the calculations.

Table 3. Calculated *CASSCF-RASSI* first-excitation energy (SO-E_1) and *g*-factors for the ground Kramers' doublet for Yb^{III}, Er^{III} and Dy^{III} compounds.

	SO-E_1	g_z	g_y	g_x
1	79.9	6.305	0.703	0.357
1b	211.2	7.593	0.607	0.475
1c	181.1	7.349	0.660	0.411
2	26.0	12.939	2.960	1.241
2b	50.2	14.700	0.500	0.055
2c	52.7	14.138	1.091	0.640
3	21.1	13.774	5.581	1.660
3b	148.0	19.548	0.010	0.006
3c	102.1	19.590	0.024	0.017

The g-tensor values of the ground state (Table 3) indicate that **3** is far from presenting a purely axial magnetic moment. In fact, the computed transversal magnetic moments between the connecting pairs of opposite magnetization (Figure 5) indicate a large transversal magnetic moment between the ground state Kramers' doublet for **3** (1.2 μ_B), which supports the existence of strong QTM in this compound. Moreover, **3**, presents heavily mixed states (as evidenced in the low magnetic moments) and high matrix elements of the magnetic moment connecting them. Further evidence for a large mixture of different states in the case of **3** is provided by the $(E_2-E_1)/E_1$ ratio, with values of -0.33, 72.6 and 5.6 for **3**, **3b** and **3c** respectively. E_1 and E_2 represent the first and second excited states before the state mixing of the spin-orbit coupling operator. A low $(E_2-E_1)/E_1$ ratio, such as the one obtained for **3** indicates that the first two excited states will be close in energy and both of them will mix to the ground level via the spin-orbit coupling, obtaining a heavily mixed state with low anisotropy.[34] High $(E_2-E_1)/E_1$ ratio

indicates that ground state will mostly mix through the spin-orbit operator with the first excited state, that has a similar anisotropy to the ground state,[34] resulting in a state with large magnetic anisotropy. As expected, the $(E_2-E_1)/E_1$ ratio is much larger for **3b** and **3c**, in line with their more axial ground state

This analysis explains why **3** and the Yb^{3+} (**1**, **1b**, **1c**) and Er^{3+} (**2**, **2b**, **2c**) are not SMMs at zero field. Complexes **3b** and **3c** show, however, strongly axial ground states (g_z around 19.6) with almost vanishing transversal components of *g*. In good agreement with the latter, these compounds exhibit comparatively lower matrix elements for the lower states than **3** and their patterns more closely resemble the classical double well potential picture (Figure 6 and S14 respectively). Moreover, the transversal magnetic moment between the ground state Kramers' doublet is very small in both complexes (around 10^{-3} μ_B), which suggest that QTM is almost suppressed in the ground state. All these correlated facts (easy-axis anisotropy of the Dy^{III} and small QTM) favor the slow relaxation of the magnetization and the SMM behavior observed for **3b** and **3c** at zero applied dc field (Figure S11).

It is clear from the experimental and theoretical results that the replacement in **3** of one tridentate tetrazolate ligand by a β-diketonato unit, favors SMM behavior. The rationale behind this trend will be analyzed in terms of the electrostatic repulsion of the ligand field and the orientation of the magnetic moment. In the case of **1** and **2**, the inclusion of a β-diketonato unit also favored SMM behavior, as the evidenced in the increase of the first excitation energy (E_1 in Table 3) and the lowering of the transversal components of the g-tensor of the ground state. However, this replacement did not lead to zero-field SMMs in **1b**, **1c**, **2b** and **2c**, as g_x and g_y remained significant in these cases.

The direction of the main component of the magnetic moment for compounds **3**, **3b** and **3c** are shown in Figures 5, 6 and S14 respectively. In the case of **3**, the ligand electrostatic potential map (Figure 5) presents a very broad repulsive "hemisphere" associated with the formally negative N-tetrazol ligands and a less repulsive half pointing to the neutral N-phenanthroline donor atoms, and therefore, there is not a clearly favored orientation to accommodate the oblate density of the Dy^{III} with the lowest electron repulsion with the ligands.[8b] This pattern explains why the ground state

shows a marked departure of purely axial anisotropy. The calculated matrix elements (Figure 5, right) show the predominance of the spin relaxation through tunnelling effect in the ground state (above 0.1 indicates an efficient spin relaxation mechanism).

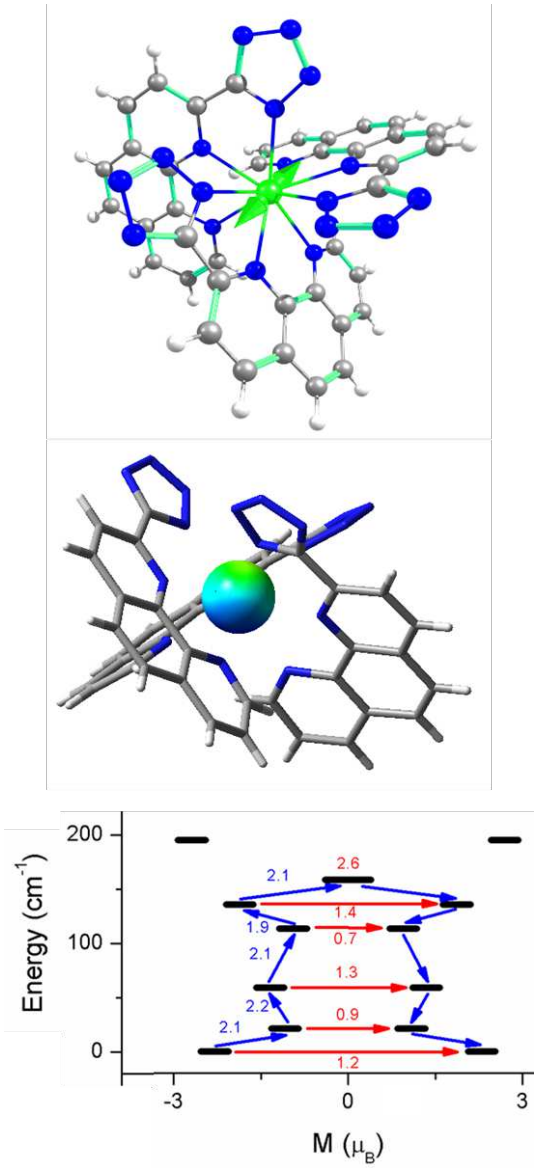

Figure 5.- Orientation of the main anisotropy axis (green arrow) for the ground Kramers' doublet of **3** (above). Electrostatic potential maps for **3**. Red and blue regions represent high and low electronic repulsive regions, respectively. The scale was adjusted to a minimum-maximum difference of 0.09 a.u. in all cases to provide comparable pictures (middle). Representation of the energy of the levels from the ground $^{6}H_{15/2}$ multiplet (y-axis) as a function of the magnetic moment of the corresponding Kramers' doublets (x-axis) for **3** (below). Matrix elements between states as a function of their magnetic moment along the main anisotropy axis are given in the

plot with arrows indicating possible magnetic relation pathways. Other pathways involving transitions between non-neighbor states are omitted for clarity.

On the other hand, the magnetic moments of **3b** and **3c** point to the negative diketonate ligands, being able to accommodate the oblate electron density in the plane perpendicular to that vector (Figures 6 and S14, respectively). In this way, the diketonate ligand helps to "pin" the magnetic moment, providing a localized repulsive region that will be avoided by the 4f electronic density. At the opposite side of the coordination sphere, we observe negative N-tetrazole ligands, roughly completing a "repulsive axis". Ligand electrostatic potential maps for **3b** and **3c** (Figures 6 and S14, respectively) display some regions of lower potential associated with formally neutral N-donor atoms on top of a more repulsive background, which is consistent with their more axial g-tensor of the ground state. The alignment of these regions does not yield a plane, preventing a complete vanishing of the transverse components of the ground g-tensor, as reflected in the perpendicular orientation of the phenanthroline fragments. As expected, the orientation of the anisotropic axis on each Dy^{III} ion calculated with the electrostatic model[35] (Figures S15) compares rather well with that obtained by the *ab initio* method. Furthermore, the matrix element between states (Figure 6, right) indicate that the probability of tunnelling effects in the ground state are very low (0.0069) being consistent with SMM behaviour found for **3b**. The fact that the experimental and calculated U_{eff} values for **3b** are larger than those of **3c** could be due to small differences between their respective Dy coordination spheres probably due to different steric effects provoked by the tmh and tta β-diketonato ligands.

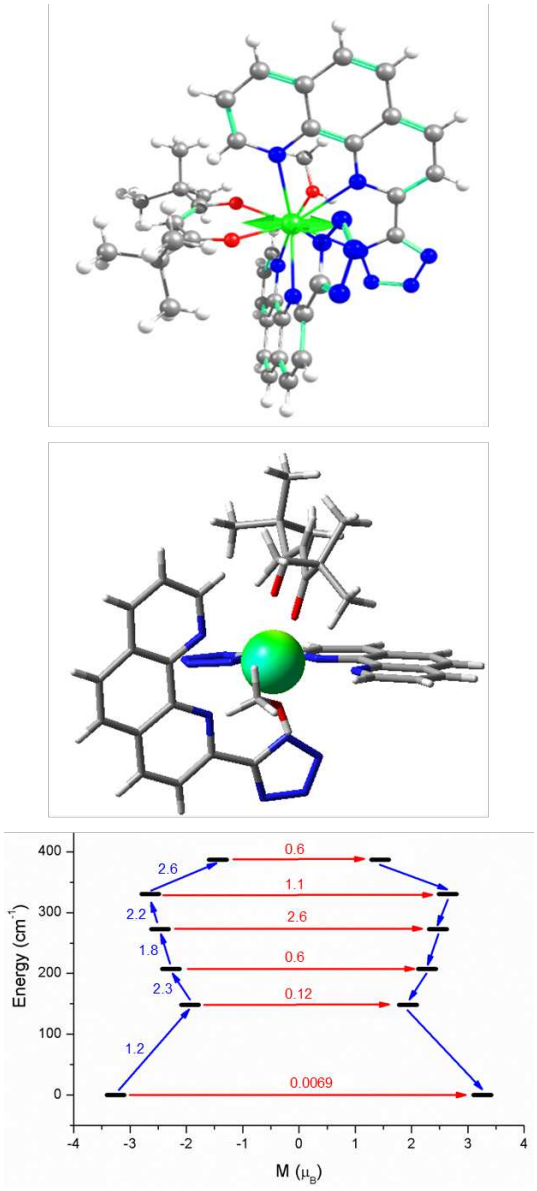

Figure 6.- Orientation of the main anisotropy axis (green arrow) for the ground Kramers' doublet of **3b** (left). Electrostatic potential maps for **3b**. Red and blue regions represent high and low electronic repulsive regions, respectively. The scale was adjusted to a minimum-maximum difference of 0.09 a.u. in all cases to provide comparable pictures (center). Representation of the energy of the levels from the ground $^{6}H_{15/2}$ multiplet (y-axis) as a function of the magnetic moment of the corresponding Kramers' doublets (x-axis) for **3b** (right). Matrix elements between states as a function of their magnetic moment along the main anisotropy axis are given in the plot with arrows indicating possible magnetic relation pathways. Other pathways involving transitions between non-neighbor states are omitted for clarity.

It should be noted at this point that, compared to **3b** and **3c**, the absence of a significant energy barrier for the reversal of the magnetization even at H_{dc} = 1000 Oe for the erbium complexes **2b** and **2c** (assuming thermal activated relaxation processes) is associated to the departure of purely easy-axis anisotropy in the ground doublet state, which can be justified using the simple oblate-prolate mode. Er^{III} has a prolate electron density distribution and, to avoid the electrostatic repulsion with the negatively charged β-diketonate oxygen atoms (those with shortest Dy-O distances and large electrostatic charge), the magnetic moment (and the f-electron cloud) should be located close to perpendicular to the shorter Er-O bonds in the mean plane of the phenanthroline nitrogen atoms and without a well-defined orientation. This leads to a large transversal component of the g-tensor, which explains the absence of a measurable relaxation barrier at zero magnetic field in **2 - 2c**. A similar argument can be applied to the Yb^{III} complexes (if a thermal activated relaxation processes is assumed), also having a prolate electron density distribution. The results obtained for the $[Ln(L)_3]$ complexes (**1-3**) and $[Ln(L)_2(\beta)]$ counterparts (**1b-3b** and **1c-3c**) clearly show the usefulness of the simple oblate-prolate electrostatic repulsion model for predicting SMM behavior in Ln^{III} mononuclear complexes.

Photophysical properties

The ability of the β-diketonate ligands to sensitize Ln^{III}-based luminescence is well known.[7] In order to determine if the ligand L^- could act as an antenna to sensitize Ln^{III}-based luminescence, the photophysical properties of the first set of complexes **1 - 5** have been studied. Firstly, to determine the inherent L-based luminescence in these complexes, the emissive properties of the gadolinium derivative **4** were investigated. UV excitation of **4** at 349 nm (Figure S16) resulted in the appearance of a very weak and structured emission band arising from the $^3\pi\pi^*$ state of the ligand with a maximum located at 545 nm with a shoulder at higher energy (484 nm). The onset of this emission band allowed the approximation in energy of the $^3\pi\pi^*$ state to be close to ~ 20500 cm^{-1}. Excitation of complex **3** at $\lambda_{ex.}$ = 349 nm did not result in the characteristic Dy ($^4F_{9/2} \rightarrow {}^6H_J$; J = 15/2, 13/2) emission which is certainly due to the fact that the energy of the donor $^3\pi\pi^*$ state is slightly lower than that of the emissive $^4F_{9/2}$ excited state of this ion. Conversely, irradiation of **5** led to the characteristic Eu^{III} emission in the red region of the visible spectrum. The emission displayed the characteristic $^5D_0 \rightarrow {}^7F_J$ transitions

dominated by the $^7F_2$ band. Bands $^7F_1$ and $^7F_4$ are moderate in intensity whereas the $^7F_3$ band is rather weak. In this case the energy gap between donor $^3\pi\pi^*$ and the acceptor ^5D_J levels (J = 0, 17230 cm^{-1}; J = 1, 19000 cm^{-1}) is ~ 3200 cm^{-1} and 1500 cm^{-1} respectively, in the optimal range to allow an efficient L → Eu^{III} energy transfer without the possibility of thermal-back energy transfer to occur. Regarding the NIR Ln^{III}-emissive properties of **1** and **2**, excitation at 355 nm resulted in the appearance of sensitized NIR emission from ions Yb^{III} ($^2F_{5/2} \rightarrow {}^2F_{7/2}$, 980 nm) and Er^{III} ($^4I_{13/2} \rightarrow {}^4I_{15/2}$, 1530 nm) respectively. Luminescence decays for these Ln^{III}-emissive samples were determined using a Nd:YAG excitation source with $\lambda_{ex.}$ = 355 nm. All the emission decays were fitted monoexponentially yielding lifetime values (Table 2) which are typical of those commonly observed for Eu^{III} (milliseconds), Yb^{III} and Er^{III} (microseconds). These values are in agreement with the absence of coordinated solvent molecules around the Ln^{III} centres.

Table 2.- Luminescence lifetime of solid-state complexes.[a]

Complex	**1**	**2**	**5**
τ/μs	11.78	2.37	$1.11 \cdot 10^3$

[a] Measured at room-temperature using $\lambda_{ex.}$ = 355 nm.

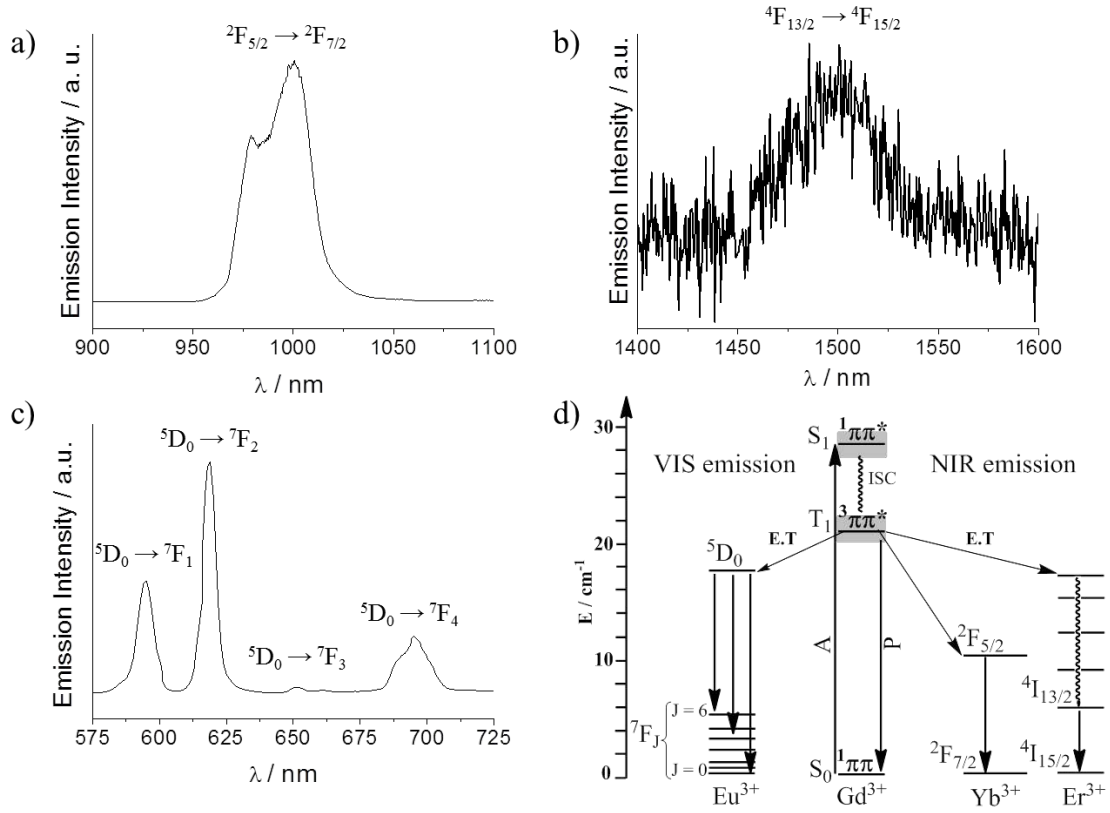

Figure 7.- Sensitized emission spectra in the solid state of complexes **1** (a), **2** (b) and **5** (c) and their respective Jablonski's diagrams (d). Approximate energy values of the singlet (S_1) and triplet (T_1) states of the ligand L were determined from the UV-vis absorption and emission spectra of complex **4**.

Conclusions

The ongoing results show that homoleptic [LnL_3] mononuclear neutral complexes, exhibiting a LnN_9 coordination sphere with a geometry close to a spherical capped square antiprism (C_{4v}), can be prepared from the reaction of the N_3-tridentate ligand 2(2*H*-tetrazol-5-yl)-1,10-phenanthroline (HL) with Ln^{III} ions. Moreover, heteroleptic [$LnL_2(\beta)$] complexes (β are the β-diketonate ligands tmh = 2,2,6,6-tetramethylheptane-3,5-dionate or tta = 2-thenoyltrifluoroacetonate) can also be obtained using the same reaction conditions as for [LnL_3] but in the presence of the corresponding β-diketonato ligand.

Dynamic *ac* magnetic studies reveal that [$DyL_2(\beta)$] complexes exhibit SMM behaviour at zero field, whereas the rest of Yb^{III}, Er^{III} and Dy^{III} complexes show field induced slow relaxation of the magnetization. In any case, the replacement of one tridentate tetrazolate ligand L^- by a β-diketonato ligand, passing from a LnN_9 to a

LnN_6O_3 coordination sphere, induces a significant increase of the thermal energy barrier. Furthermore, it seems that the U_{eff} values for the $[DyL_2(tmh)]$ complexes are larger than those for the $[DyL_2(tmh)]$ counterparts. These observations are supported by CASSCF-RASSI theoretical studies, as they indicate that: (i) U_{eff} $[DyL_3]$ << U_{eff} $[DyL_2(tta)]$ < U_{eff} $[DyL_2(tmh)]$ and (ii) the ground Kramer's doublet for $[DyL_3]$ is far from being Ising type and exhibits significant QTM, whereas $[DyL_2(\beta)]$ complexes present a strongly axial ground Kramer's doublet with almost suppressed QTM. These results explain why $[DyL_2(\beta)]$ complexes show SMM behaviour at zero field and, however, the complex $[DyL_3]$ needs the application of a dc field to observe slow relaxation of the magnetization. This fact can also be justified by taking into account the effect of the repulsion of the ligand field on the orientation of the magnetic moment. Thus, for the $[DyL_3]$ the tetrazolate nitrogen atoms bearing the large negative charge are located at the same side of the Dy^{III} ion, giving rise to a broad negative region, so that there is not a clearly favoured orientation for the magnetic moment and the ground Kramer's doublet show a marked departure from pure axial anisotropy. However, for the $[DyL_2(\beta)]$ complexes, the tetrazolate nitrogen atoms and the diketonate oxygen atoms (those bearing larger negative charge) are located at opposite sides of the Dy^{III} ion, completing a repulsive axis and giving rise to axial ground state with the magnetic moment oriented along the repulsive axis (the oblate electron shape distribution is perpendicular to this axis to avoid repulsion). The behaviour of **1-1c** and **2-2c** also follows the same trend, although showing a larger transverse component of the g-tensor for the ground state. The latter enhances the tunnelling mechanism of magnetic relaxation, requiring and external field to measure a relaxation barrier. These results demonstrate the utility of the oblate-prolate repulsion model to predict SMM behaviour in Ln^{III} mononuclear complexes.

Finally, the photoluminescence study of the $[Ln(L)_3]$ complexes demonstrated the ability of the ligand L^- to sensitize Yb^{III}, Er^{III} and Eu^{III}-based emissions in the respective NIR and visible spectroscopic regions, with lifetime values that are in agreement with the absence of coordinated solvent molecules in the Ln^{III} coordination sphere.

Acknowledgments

E.C., J.M.H. and I.D.O. are thankful for financial support to Ministerio de Economía y Competitividad (MINECO) for Project CTQ2014-56312-P, the Junta de Andalucía (FQM-195 and the Project of excellence P11-FQM-7756) and the University of Granada. E. R is grateful to MINECO (Project CTQ2015-64579-C3-1-P) and the *Generalitat de Catalunya* for an ICREA Academia award. D.A. thanks CONICYT+PAI "Concurso nacional de apoyo al retorno de investigadores/as desde el extranjero, convocatoria 2014 82140014". We thank the CSUC, Universitat de Barcelona, for computational resources. Cardiff University is thanked for support (S.J.A.P.).

Supporting Information Available

Elemental analyses shape measures, tables of selected bond lengths and distances, crystallographic data and dc and ac magnetic data. Crystallographic data (excluding structure factors) for the structures in this paper have been deposited with the Cambridge Crystallographic Data Centre as supplementary publication numbers CCDC 1469025-1469037. Copies of the data can be obtained, free of charge, on application to CCDC, 12 Union Road, Cambridge CB2 1EZ, U.K.: http://www.ccdc.cam.ac.uk/cgi-bin/catreq.cgi , e-mail: data_request@ccdc.cam.ac.uk, or fax: +44 1223 336033.

References

1.- a) H. Zhao, Z.-R. Qu, H.-Y. Ye, R.-G. Xiong, *Chem. Soc. Rev.*, **2008**, *37*, 84-100; b) G. Aromí, L. A. Barrios, O. Roubeau, P. Gamez, *Coord. Chem. Rev.,* **2011**, *255 (5–6)*, 485–546; c) E. A. Popova, R. E. Trifonov, Vladimir A. Ostrovskii, *ARKIVOC* **2012**, *1*, *Reviews and Accounts*, 45-65.

2.- W. G. Finnegan, R. A. Henry, R. Lofquist, *J. Am. Chem. Soc.,* **1958,** *80,* 3908-3911.

3.- a) S. Vorona, T. Artamonova, Y. Zevatskii, L. Myznikov, *Synthesis,* **2014,** *46,* 781-786; b) J. Roh, K. Vavrova, A. Hrabalek, *Eur. J. Org. Chem.,* **2012,** *31,* 6101-6118; c) Z. P. Demko, B. K. Sharpless, *J. Org. Chem.,* **2001,** *66,* 7945-7950.

4.- A. J. Mota, A. Rodríguez-Diéguez, M. A. Palacios, J. M. Herrera, D. Luneau, E. Colacio, *Inorg. Chem.* **2010,** *49,* 8986-8996 and references therein.

5.- a) Q. –Y. Li, F. Zhou, C. Zhai, L. Shen, X.-Y. Tang, J. Yang, G.-W.Yang, Z.-F. Miao, *Inorg. Chem. Commun.,* **2011,** *14,* 843-847; b) Q.-L.Song, B.-Q.Guo, W. Zhang, P. Lan, P., S. Ping-Hua, C. Wei-Min, *The Journal of Antibiotics,* **2011,** *64,* 571-581.

6.- a) M. Giraud, E. S. Andreiadis, A. S. Fisyuk, R. Demadrille, J. Pecaut, D. Imbert, M. Mazzanti, *Inorg. Chem.* **2008,** *47,* 3952-3954; b) E. S. Andreiadis, R. Demadrille, D. Imbert, J. Pecaut and M. Mazzanti, *Chem. –Eur. J.,* **2009,** *15,* 9458-9476; c) E. S. Andreiadis, D. Imbert, J. Pecaut, R. Demadrille, M. Mazzanti, *Dalton Trans.,* **2012,** *41,* 1268-1277; d) G. Bozoklu, C. Marchal, J. Pecaut, D. Imbert, M. Mazzanti, *Dalton Trans.,* **2010,** *39,* 9112-9122; e) N. M. Shavaleev, S. V. Eliseeva, R. Scopelliti, J. -C. G. Bünzli, *Inorg. Chem.,* **2014,** *53,* 5171-5178; f) S. Di Pietro, D. Imbert, M. Mazzanti, *Chem. Commun.,* **2014,** *50,* 10323-10326; g) S. Mal, M. Pietraskiewicz, O. Pietraskiewicz, *J. Coord. Chem.,* **2015,** *68,* 367-377.

7.- a) M. D. Ward, *Coord. Chem. Rev.* **2007**, *251*, 1663-1677; b) K. Binnemans, *Chem. Rev*. **2009**, *109*, 4283-4374; c) J.-C. G. Bünzli, *Acc. Chem. Res*. **2006**, *39*, 53-61; d) W. C. Chan, D. J. Maxwell, X. Gao, R. E. Bailey, M. Han, S. Nie, *Curr. Opin. Biotechnol.* **2002**, *13*, 40-46; e) P. Hänninen, H. Härmä (Eds), *Lanthanide Luminescence, Photophysical, Analytical and Biological Aspects*, Springer-Verlag, Berlin-Hei delberg, **2011**; f) Atwood, D. Ed. *The rare Elements: Fundamental and applications*, John Wiley and Sons, **2012**.

8.- a) R. A. Layfield, M. Murugesu (eds), *Lanthanides and Actinides in Molecular Magnetism*, Wiley-VCH, Weinheim, Germany, **2015**; b) J. D. Rinehart, J. R. Long, *Chem. Sci.* **2011**, *2*, 2078-2085.

9.- a) D. Gatteschi, R. Sessoli, *Angew. Chem., Int. Ed.* **2003**, *42*, 268-297. a) Y. N. Guo, G. F. Xu, Y. Guo, J. Tang, *Dalton Trans.* **2011**, *40*, 9953-9963; b) L. Sorace, C. Benelli, D. Gatteschi, *Chem. Soc. Rev*. **2011**, *40*, 3092-3104; c) J. Luzon, R. Sessoli, *Dalton Trans*. **2012**, *41*, 13556-13567; d) J. M. Clemente-Juan, E. Coronado, A. Gaita-Ariño, *Chem. Soc. Rev.* **2012**, *41*, 7464-7478; e) D. N. Woodruff, R. E. P Winpenny, R. A.

Layfield, *Chem. Rev*. **2013**, *113*, 5110-5148; h) P. Zhang, Y.-N. Guo, J. Tang, *Coord. Chem. Rev.* **2013**, *257*, 1728-1763; f) F. Habib, M. Murugesu, *Chem. Soc. Rev.* **2013**, *42*, 3278-3288; g) R. A. Layfield, *Organometallics* **2014**, *33*, 1084-1099; h) B. W. Wang, S. Gao in *The Rare Earth Elements, Fundamental and Applications*, (Ed: D. A. Atwood), John Wiley and Sons, **2012**, 153-160; (i) J. Tang, P. Zhang, in *Lanthanide Single Molecule Magnets*, Springer-Verlag, Berlin Heidelberg, **2015**; (j) F. Luis, J. F. Fernández in *Molecular Magnets: Physics and Applications* (Ed. J. Bartolomé), Springer-Verlag, Berlin Heidelberg, **2014**.

10.- L. Bogani, W. Wernsdorfer, *Nat. Mat.* **2008**, *7*, 179-186.

11.-a) A. R. Rocha, V. M. García-Suárez, S. W. Bailey, C. J. Lambert, J. Ferrerand, S. Sanvito, *Nat. Mater.* **2005**, *4*, 335-339; b) M. Affronte, *J. Mater. Chem*. **2009**, *19*, 1731-1737.

12.- a) M. N. Leuenberger, D. Loss, *Nature*, **2001**, *410,* 789-793; b) A. Ardavan, O. Rival, J. J. L. Morton, S. J. Blundell, A. M. Tyryshkin, G. A. Timco, R. E. P. Winpenny, *Phys. Rev. Lett.*, **2007**, *98*, 057201/1-057201/4; c) P. C. E. Stamp, A. Gaita-Ariño, *J. Mater. Chem*. **2009**, *19*, 1718-1730.

13.- a) R. Sessoli and A. K. Powell, *Coord. Chem. Rev.*, **2009**, *253*, 2328-2341; b) M. Andruh, J. P. Costes, C. Diaz and S. Gao, *Inorg. Chem*., **2009**, *48*, 3342-3359; c) "Molecular Magnets", themed issue (Ed.: E. K. Brechin), *Dalton Trans*., **2010**, ***20***; d) M. Andruh, *Chem. Commun*., **2011**, *47*, 3025-3042.

14.- a) J. J. Le Roy, M. Jeletic, S. I. Gorelsky, I. Korobkov, L. Ungur, L. F. Chibotaru, M. Murugesu, *J. Am. Chem. Soc.* **2013**, *135*, 3502−3510; b) S. Jiang, B.-W. Wang, H.-L. Sun, Z.-M. Wang, S. Gao, *J. Am. Chem. Soc*. **2011**, *133*, 4730–4733.

15.- a) J. D. Rinehart, M. Fang, W. J. Evans, J. R. Long, *Nature Chem.* **2011**, *3*, 538-542; b) J. D. Rinehart, M. Fang, W. J. Evans, J. R. Long, *J. Am. Chem. Soc.* **2011**, *133*, 14236-14239.

16.- F. Tuna, C. A. Smith, M. Bodensteiner, L. Ungur, L. F. Chibotaru, E. J. L. McInnes, R. E. P. Winpenny, D. Collison, R. A. Layfield, *Angew. Chem., Int. Ed.* **2012**, *51*, 6976-6980.

17.- a) T. Pugh, F. Tuna, L. Ungur, D. Collison, E. J.L. McInnes, L. F. Chibotaru, R. A. Layfield, *Nat. Commun.* **2015**, *6*, 7492-7500. b) T. Pugh, V. Vieru, L. Chibotaru, R. A. Layfield, *Chem. Sci.*, **2016**, *7*, 2128-2137.

18.- a) G. J. Chen, C. Y. Gao, J. L. Tian, J. K. Tang, W. Gu, X. Liu, S. P. Yan, D. Z. Liao, P. Cheng, *Dalton Trans.*, **2011**, *40*, 5579−5583. b) G. Chen, Y. Guo, J. Tian, J. Tang, W. Gu, X. Liu, S. Yan, P. Cheng, D. Z. Liao, *Chem. Eur. J.* **2012**, *18*, 2484−2487. c) W. Yu, F. Schramm , E. Moreno Pineda, Y. Lan, O. Fuhr , J. Chen, H. Isshiki, W. Wernsdorfer, W. Wulfhekel, M. Ruben, *Beilstein J. Nanotechnol*. **2016**, 7, 126–137. d) J. Zhu, C. Wang, F. Luan, T. Liu, P. Yan, and G. Li, *Inorg. Chem*. **2014**, 53, 8895−8901 and references therein. e) Y. Dong, P. Yan, X. Zou, T. Liua, G. Li , *J. Mater. Chem. C*, **2015**, 3, 4407-4415.

19.- a) E. L. Gavey, Y. Beldjoudi, J. M. Rawson, T. C. Stamatatos, M. Pilkington, *Chem. Commun.*, **2014**, *50*, 3741-3743. b) U. J. Williams, B. D. Mahoney, P. T. DeGregorio, P. J. Carroll, E. Nakamaru-Ogiso, J. M. Kikkawa, E. J. Schelter, *Chem. Commun.*, **2012**, *48*, 5593-5595.

20.- W. Zhang , F. Zhao , T. Liu , M. Yuan , Z.-M. Wang, S. Gao, *Inorg. Chem.* **2007**, *46*, 2541-2555.

21.- O. V. Dolomanov, L. J. Bourhis, R. J. Gildea, J. A. K. Howard, and H. Puschmann, "OLEX2: a complete structure solution, refinement and analysis program," *Journal of Applied Crystallography*, **2009**, *42*, 339–341.

22.- G. M. Sheldrick, "A short history of SHELX," *Acta Crystallographica A*, **2008**, *64*, 112–122.

23.- F. Aquilante, L. De Vico, N. Ferré, G. Ghigo, P. A. Malmqvist, P. Neogrády, T. B. Pedersen, M. Pitoňák, M. Reiher,B.O. Roos, L. Serrano-Andrés, M. Urban, V. Veryazov, R. Lindh, *J. Comput. Chem*. **2010**, *31*, 224-247.

24.- L. F. Chibotaru and L. J. Ungur, *Chem. Phys.* **2012**, *137*, 064112-064122.

25.- A. D. Becke, *J. Chem. Phys.* **1993**, *98*, 5648-5652.

26.- A. Schaefer, C. Huber, and R. Ahlrichs, *J. Chem. Phys.* **1994**, *100*, 5829-5835.

27.- M. J. Frisch, G. W. Trucks, H. B. Schlegel, G. E. Scuseria, M. A. Robb, J. R. Cheeseman, G. Scalmani, V. Barone, B. Mennucci, G. A. Petersson, H. Nakatsuji, M. Caricato, X. Li, H. P. Hratchian, A. F. Izmaylov, J. Bloino, G. Zheng, J. L. Sonnenberg, M. Hada, M. Ehara, K. Toyota, R. Fukuda, J. Hasegawa, M. Ishida, T. Nakajima, Y. Honda, O. Kitao, H. Nakai, T. Vreven, J. A. Montgomery, Jr., J. E. Peralta, F. Ogliaro, M. Bearpark, J. J. Heyd, E. Brothers, K. N. Kudin, V. N. Staroverov, R. Kobayashi, J. Normand, K. Raghavachari, A. Rendell, J. C. Burant, S. S. Iyengar, J. Tomasi, M. Cossi, N. Rega, J. M. Millam, M. Klene, J. E. Knox, J. B. Cross, V. Bakken, C. Adamo, J. Jaramillo, R. Gomperts, R. E. Stratmann, O. Yazyev, A. J. Austin, R. Cammi, C. Pomelli, J. W. Ochterski, R. L. Martin, K. Morokuma, V. G. Zakrzewski, G. A. Voth, P. Salvador, J. J. Dannenberg, S. Dapprich, A. D. Daniels, Ö. Farkas, J. B. Foresman, J. V. Ortiz, J. Cioslowski, and D. J. Fox, Gaussian, Inc., Wallingford CT, **2009**.

28.- M. Llunell, D. Casanova, J. Cirera, J. M. Bofill, P. Alemany, S.Alvarez, M. Pinsky, D. Avnir, *SHAPE v1.1b*, Barcelona (Spain), **2005**.

29.- a) I. Oyarzabal, J. Ruiz, E. Ruiz, E., D. Aravena, J. M. Seco, E. Colacio, *Chem. Commun*. **2015**, *51*, 12353-12356; b) J. P. Costes, S. Titos-Padilla, I. Oyarzabal, T. Gupta, C. Duhayon, G. Rajaraman, E. Colacio, *Chem. Eur. J.* **2015**, *21*, 15785-15796; c) H. L. C. Feltham, Y. Lan, F. Klöwer, L. Ungur, L. F. Chibotaru, A. K. Powell, S. Brooker, *Chem. Eur. J.* **2011**, *17*, 4362-4365; d) Y. Bi, Y.-N. Guo, L. Zhao, Y. Guo, S.-Y. Lin, S. D. Jiang, J. Tang, B. W. Wang, S. Gao, *Chem. Eur. J.* **2011**, *17*, 12476-12481 and references therein.

30.- a) J. L. Liu, K. Yuan, J. D. Leng, L. Ungur, W. Wernsdorfer, F. S. Guo, L. F. Chibotaru, M. L. Tong, Inorg. Chem. **2012**, *51*, 8538-8544; b) P. H. Lin, W. B. Sun, Y. M. Tian, P. F. Yan, L. Ungur, L. F. Chibotaru, M. Murugesu, Dalton Trans. **2012**, *41*, 12349-12352; c) J. D. Leng, J. L. Liu, Y. Z. Zheng, L. Ungur, L.F. Chibotaru, F. S. Guo, M. L. Tong, *Chem. Commun.* **2013**, *49*, 158-160; d) Q. W.Li, J. L. Liu, J. H. Jia, J. D. Leng, W. Q. Lin, Y. C. Chen, M. L. Tong, *Dalton Trans.* **2013**, *42*, 11262-11270; e) F. Pointillart, B. Le Guennic, S. Golhen, O. Cador, O. Maury, L. Ouahab, *Chem. Commun.* **2013**, *49*, 615-617; f) J. Ruiz, G. Lorusso, M. Evangelisti, E. K. Brechin, S. J. A. Pope, E. Colacio, *Inorg. Chem.* **2014**, *53*, 3586-3594.

31.- A. Abragam, B. Bleaney, *Electron Paramagnetic Resonance of Transition Ions*, Clarendon Press, Oxford, **1970**.

32.- K. N. Shirivastava, *Phys. Status Solidi B*, **1983**, *117*, 437-458.

33.- K. Qian, J. J. Baldovi, S.-D. Jiang, A. Gaita-Arino, Y.-Q. Zhang, J. Overgaard, B.-W. Wang, E. Coronado, S. Gao, *Chem. Sci.*, **2015**, *6*, 4587-4593.

34.- D. Aravena, E. Ruiz, *Inorg. Chem.* **2013**, *52*, 13770−13778.

35.- N. F. Chilton, D. Collison, E. J. L. McInnes, R. E. P. Winpenny, A. Soncini, *Nat. Commun*. **2013**, *4*, 2551

TOC

FULL PAPER

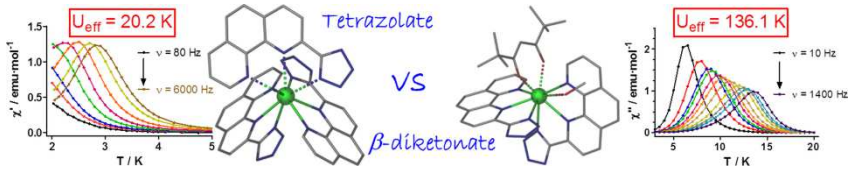

Increasing U_{eff} in Ln(III)-based single-ion magnets by ligand replacement. Mononuclear LnL_3 complexes prepared from a tridentate phenanthroline-tetrazolate ligand display field-induced SMM behaviour with very low thermal energy barriers. The replacement of one tridentate phenanthroline-tetrazolate ligand by a β-diketonate, induces a significant increase of U_{eff} and leads to these new complexes to behave as SMMs at zero field.

Juan-Ramón Jiménez, Ismael F. Díaz-Ortega, Eliseo Ruiz, Daniel Aravena, Simon J. A. Pope, Enrique Colacio* and Juan Manuel Herrera*.*

Page No. – Page No.

Lanthanide-Tetrazolate Complexes Combining SIM and Luminescent Properties. The Effect of the Replacement of N_3-tetrazolate by β-Diketonate Ligands on the anisotropy energy barrier